eXPRESS Polymer Letters Vol.14, No.6 (2020) 566–575
Available online at www.expresspolymlett.com
https://doi.org/10.3144/expresspolymlett.2020.46

Bending control of liquid-crystal elastomers based on doped azo derivatives synthesized via controlled gradient polymerization

S. Fitriyani[1], *C. Y. Liu*[2], *Y. H. Hung*[1], *Y. S. Zhang*[1], *J. H. Liu*[1*]

[1]Department of Chemical Engineering, National Cheng Kung University, 70101 Tainan, Taiwan
[2]Department of Materials Science and Engineering, National Cheng Kung University, 70101 Tainan, Taiwan

Received 20 August 2019; accepted in revised form 11 October 2019

Abstract. The intelligence, complexity, and diversification of nature is a continuous source of inspiration for humankind. Imitating natural intelligence to devise bionic microrobots with self-regulated features remains an enormous challenge. Herein, we demonstrate a biomimetic soft material that uses light to trigger mechanical motion. This light-sensitive mimosa mimetic film was designed based on liquid crystal elastomers (LCEs) and photoisomerizable azo compounds. To control the bending direction, a predesigned UV-induced gradient polymerization was used. The energy-controlled polymerized film comprises one high-density and one low-density liquid crystal mesogen face. Similar to mimosas, the fabricated films achieved stimuli-responsive actuation, exhibiting shape deformation upon light illumination. The elastic network undergoes reversible shape changes via photochemical trans-cis isomerization of an azo compound in response to a stimulus. In this study, only a small amount of photoisomerizable 1-Hydroxy-*n*-(4-nitro-azobenzene-4′-oxy)hexane (**AZO**) was used; however, the domino effect caused a significant reversible actuation. The mesogen density of the top and bottom faces was found to be an important factor for the bending control. This study explores a new way to fabricate films that can bend in controlled directions during light irradiation. This phototunable film is expected to be used for applications in microrobotics and micromachinery.

Keywords: *smart polymers, liquid crystal elastomers, azo derivatives, photopolymerization*

1. Introduction

Nature is an infinite source of inspiration for numerous astonishing instances of biomimetic research [1]. For thousands of years, from self-assembly to morphological control of different dimensions, scales, and functions to sophisticated mechanical locomotion and autonomous sensing strains, humans have continuously learned from biomimicry research, thus creating modern civilization [2–6]. However, mimicking the intelligence of native species in artificial systems, that is, achieving bionic actuators capable of self-regulation and self-action and systems that can autonomously distinguish different targets and adapt to unexpected environmental changes, remains a long-standing challenge [7–11]. To date, research on electronically driven artificial intelligence devices that rely on computer program control has grown substantially. However, the incorporation of complex computing circuitry, power sources and electrically driven actuators into miniaturized robotic systems to respond to natural stimulation (*e.g.*, temperature, light, and humidity) requires massive data support. Taking advantage of materials that sense environmental changes as part of the design of artificial intelligence actuators is a mainstream research direction of the future [12–14].

*Corresponding author, e-mail: jhliu@mail.ncku.edu.tw

Biomimetic materials are synthetic materials that mimic natural materials or that follow a design motif derived from nature [15–18]. This nascent field has made significant developments in recent years. Studies of ordered phenomena in simple systems can be adapted to more complex cases found in soft matter-based actuator materials. These materials have attracted widespread attention due to their ability to undergo dramatic bending, folding or twisting in response to a large variety of external stimuli [19–23]. Among the different stimuli, light has fascinated scientists because it is a clean, contactless energy source with unique properties (wavelength, intensity, polarization), especially in light-responsive liquid-crystal elastomers (LCEs), which are smart materials that can exhibit large shape deformations upon illumination [24–27]. In nature, plants can convert simple environmental stimuli into various mechanical motions [28, 29]. For example, incoming light deactivates auxin on the light side of a plant, allowing the shaded part to continue growing and eventually bending the plant towards the light. To the best of our knowledge, light-responsive LCEs can be synthesized by copolymerization of light-active monomers or blended light-active dopants into a polymer matrix [30, 31]. The elastic matrix comprises a loosely cross-linked network of liquid crystalline moieties with controlled molecular alignment that can undergo reversible shape changes in response to a photochemical cis-trans isomerization reaction [32, 33]. Unlike conventional electronically controlled mechanical microdevices, LCE-based organic devices provide natural safety and human-friendly contact.

In our previous article [34], we reported a novel method for the fabrication of gradient refractive index (GRIN) plastic lenses using a sloped UV lamp via an energy-controlled process [35]. This concept was used in this study for the fabrication of polymer density-controlled LCE films. To control the bending direction, many studies have used pretreated perpendicular- and parallel-aligned layers for the fabrication of liquid-crystal films. In this study, we developed an intelligent optomechanical mimosa-mimetic film based on a liquid-crystal elastomer monolith with a gradient polymer density, which can autonomously open and close by responding to incident light without any need for external control circuitry. In essence, light-induced actuation is based on controlling the polymer density within the liquid-crystal polymer network via UV gradient energy [34]. During UV polymerization of the precursor substrate, the top layer is closer to the UV lamp than the bottom side is. Light absorption by the **AZO** compound continuously occurs in the direction of the film thickness. Furthermore, the reaction rate differences between liquid-crystal monomers cause polymer component variations in the film thickness. As a result, gradient polymer density films are fabricated due to the reaction rate differences between the cross-linker and monomer and between the **AZO** absorption and decrease in light energy gradient. The results observed in this study open a new route to fabricate films that bend in controlled directions during light irradiation.

2. Experimental

2.1. Instruments

Fourier transform infrared (FTIR) spectra were recorded on a Jasco VALOR III (Tokyo, Japan) Fourier transform infrared spectrophotometer. Nuclear magnetic resonance (NMR) spectra were obtained using a Bruker AMX-500 high-resolution NMR spectrometer. Differential scanning calorimetry (DSC) was conducted on a Perkin-Elmer DSC 7 system in a nitrogen atmosphere with heating and cooling rates of +5 and –5 °C·min^{-1}, respectively. The morphologies of the samples were characterized by scanning electron microscopy (SEM) microphotographs with a JEOL HR-FESEM JSM-6700F (Osaka, Japan) instrument. UV spectroscopy measurements were carried out with a Jasco V-550 UV-VIS spectrophotometer. Dynamic mechanical analysis was measured with an RSA-G2 TA instrument.

2.2. Chemicals and reagents

Analytical-grade chemicals and solvents were used as received without further purification. Nematic LC RM105 monomer and RM257 cross-linker were purchased from Merck (Darmstadt, Germany). RM257 shows a nematic phase from 70 to 125 °C in the heating cycle. The photoinitiator Irgacure-369 was obtained from Ciba Specialty Chemicals. To make the mixture responsive to visible light, a synthesized photoisomerizable **AZO** dye was doped into the liquid crystal mixture. The **AZO** dye 1-hydroxy-*n*-(4-nitro-azobenzene-4′-oxy)hexane was synthesized following the processes shown in Figure 1. 4-Nitroaniline, 6-chloro-1-hexanol, $NaNO_2$, and *N*,*N*-dimethylacetamide were purchased from Acros Chemical Company. The chemical structures of RM105, RM257, **AZO**, and Irgacure-369 are shown in

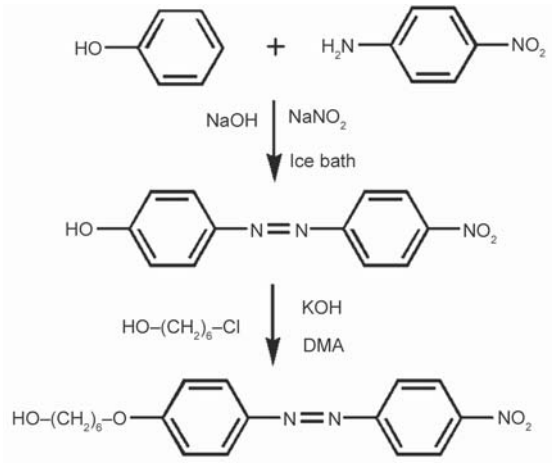

Figure 1. Synthesis of 1-hydroxy-*n*-(4-nitro-azobenzene-4′-oxy)hexane (**AZO**).

Figure 1. Photo alignment reagent SD1 was purchased from Dainippon Ink and Chemicals Ltd.

2.3. Synthesis of chemicals

2.3.1. 1-Hydroxy-4′-nitro-azobenzene

4-Nitroaniline (5 g, 36.23 mmol) was dissolved in 1 M aqueous HCl (100 mL) and kept in an ice bath at 0 °C. $NaNO_2$ (3.53 g, 51.16 mmol) in water (20 mL) was added dropwise to the former solution and stirred for 30 min. NaOH (4.4 g, 0.11 mol) and phenol (5.0 g, 53.19 mmol) were dissolved in water (100 mL) and stirred for 30 min at 0 °C. The former solution was added dropwise to the latter solution at 0 °C and then stirred for 1 h. The resulting mixture was poured into water, and the solution was neutralized with 5% aqueous HCl. The crude product was filtered and recrystallized twice by using EtOH. Yield: 6.0 g (68.1%).

FT-IR (KBr, ν_{max} [cm^{-1}]: 1510 (NO_2), 3450 (OH). ^{1}H-NMR ($CDCl_3$, δ [ppm]): 5.60 (s, 1H, –OH), 6.97–7.00 (d, 2H, Ar–H), 7.92–7.97 (d, 4H, Ar–H), 8.35–8.37 (d, 2H, Ar–H).

2.3.2. 1-Hydroxy-*n*-(4-nitro-azobenzene-4′-oxy) hexane (AZO)

4-Hydroxy-4′-nitro-azobenzene (4.0 g, 16.50 mmol) was dissolved in *N*,*N*-dimethylacetamide (150 mL). KOH (1.1 g, 19.8 mmol) dissolved in *N*,*N*-dimethylacetamide (30 mL) was then added dropwise to the former solution. 6-Chloro-1-hexanol (14.5 g, 103.9 mmol) and a trace amount of KI were then added, and the solution was heated at reflux for 30 h. The resulting mixture was poured into water and extracted with CH_2Cl_2. After drying, the crude product was recrystallized twice from ethanol. Yield: 3.22 g (57%). Figure 1 shows the synthetic process of **AZO**. The synthesized **AZO** was confirmed using ^{1}H-NMR and FTIR.

2.4. Fabrication of sample cells

SD1 purchased from Dainippon Ink and Chemicals Ltd. was used as the photoalignment material because the intermolecular forces between SD1 and LCEs are not strong. Thus, it is easy to separate and maintain the integrity of the LCEs after polymerization. The preparation of the sample film is shown in Figure 2. To obtain a parallel-aligned liquid crystal cell, polarized light (365 nm) was used to polymerize the azobenzene-based photoalignment layer SD1 coated on cell substrates. Based on the polarized light, SD1 molecules were aligned perpendicular to the polarized light, as shown in Figure 2a. The sample cell was fabricated by applying a 23 μm spacer in parallel with the alignment layer-treated substrates. As shown in Figure 2a, the LC mixture in the sample cell was irradiated with UV light leads to the formation of LC sample films.

3. Results and discussion

3.1. Synthesis of LCEs

Photoaligning SD1 (Dainippon Ink and Chemicals Ltd.) was used as the alignment layer coated on the substrates. UV light (365 nm) was used as the light source for the alignment. Figure 2a shows the UV-aligning exposure setup. During UV irradiation, SD1 molecules align in a direction perpendicular to the exposure plane of the polarized light. The alignment of the UV-induced aligning layer on the substrate was confirmed using crossed polarizers. A liquid-crystal cell was prepared using two parallel, pretreated substrates with 23 μm spacers. Photopolymerization was carried out at 45 °C, at which point the mixture forms a nematic liquid-crystal phase. As illustrated in Figure 2b, a precursor substrate containing liquid-crystal mixtures was exposed to UV light. It is well known that light energy decreases dramatically with increasing distance from a light source. Due to the film thickness, **AZO** absorption, and reaction rate differences between the cross-linker and monomer, a gradient polymer density film was observed. Theoretically, polymerization of the top layer is faster than that of the bottom side, forming a distribution gradient in polymer density. The polymer densities on the top and bottom sides were confirmed using SEM. A mixture of 75 mol% monomer RM105,

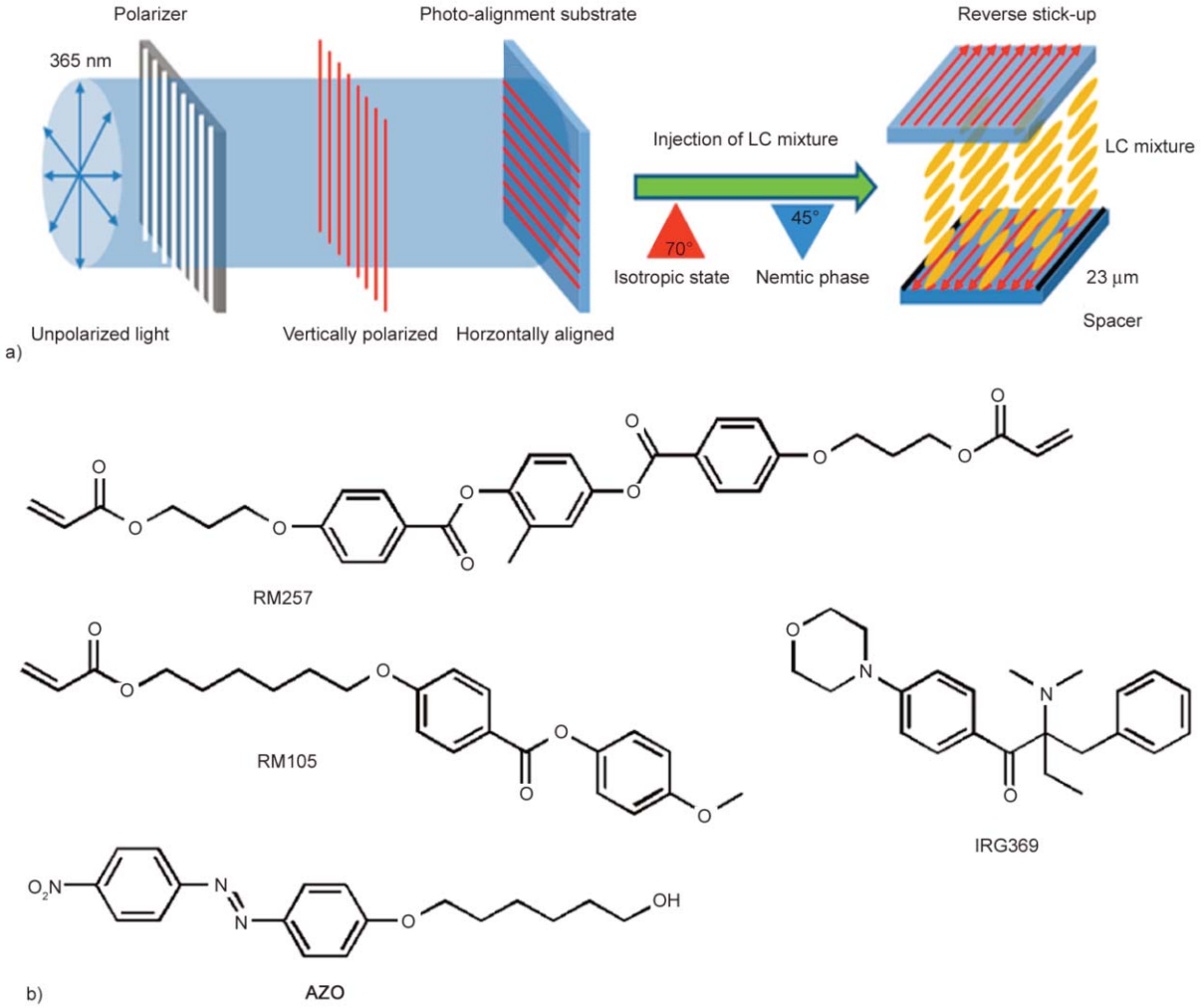

Figure 2. Schematic representations of (a) alignment layer treatment and (b) structures of the chemicals used.

20 mol% diacrylate cross-linker RM257 and 1 mol% photoinitiator IRG369 was used for the fabrication of a liquid-crystal elastomer. To make the mixture responsive to visible light, a synthesized photoisomerizable **AZO** dye (4 mol%) was doped into the liquid crystal mixture. The synthetic process of the **AZO** dye is shown in Figure 1. Under visible light exposure, **AZO** shows reversible trans-cis isomerization. Figure 2b shows the chemical structure of the compounds used in this work. The UV intensity was controlled by changing the distance between the sample cell and UV light source. As shown in Figure 3a, the sample cell was exposed to an energy distribution gradient. After 4 h of UV curing, the sample cell was opened, and the synthesized film was cut into strips or mimosa-like shapes. After polymerization, the polymer film shows elastic properties at room temperature. The stress-strain and thermogram of the synthesized liquid crystal elastomer were confirmed using dynamic mechanical analyzer (DMA) and DSC, respectively.

3.2. Bending control of LCEs

Based on the gradient UV light exposure, as shown in Figure 3a, the polymer density of the top layer is greater than that of the bottom layer. The results were confirmed by the SEM morphologies of the front and rear sides of the fabricated LCE film, showing the density difference between the sides. Figure 3a shows a schematic illustration of the density difference of the polymerized LCE film due to gradient UV energy exposure. For LC molecules that are parallel in the longer length of the film, as shown in Figure 3b, UV exposure leads to bending from the front to the rear side. As shown in Figure 3c, for the higher-density front side, the **AZO** variation is restricted. However, trans-cis isomerization induced by UV exposure disturbs the lower-density rear side. Due to the molecular order variation of the liquid crystal molecules, as shown in Figure 3c, a decrease in the rear side length leads to the occurrence of bending. Theoretically, after stimulus UV exposure, a decrease in the molecular order

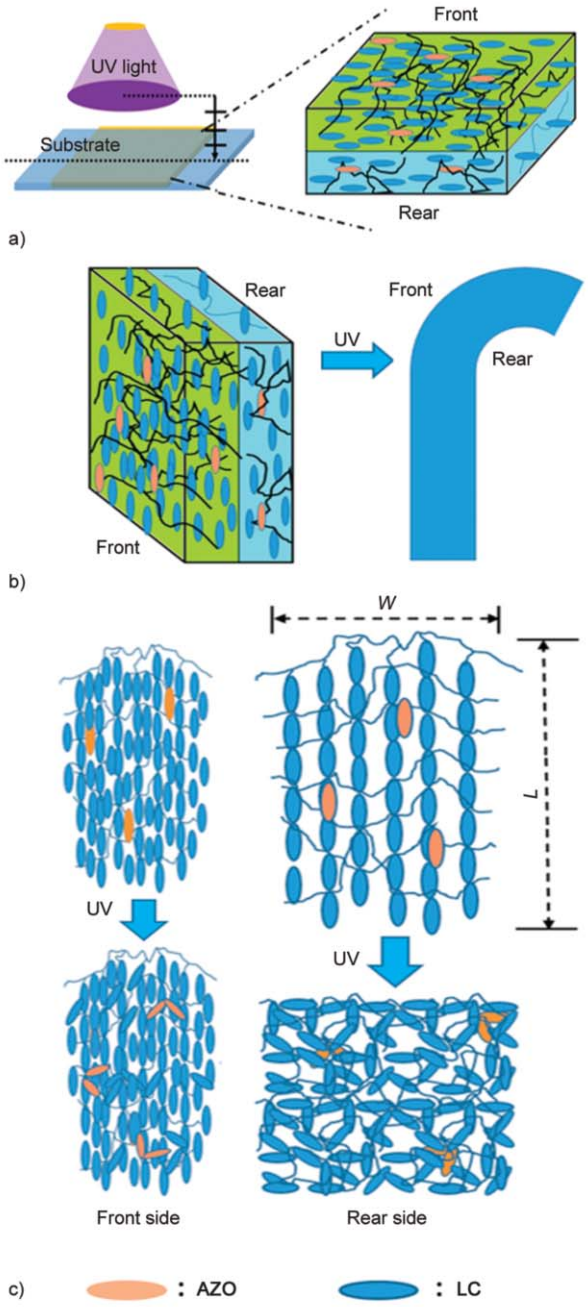

Figure 3. (a) Polymerization of liquid crystal monomers, (b) the synthesized film bent to the rear side during UV irradiation, and (c) illustration of the trans-cis disturbing effect.

from the LC phase to an isotropic random phase decreases the length '*L*'.

In contrast to these phenomena, in the case of LC molecules parallel in the short length of the film, as shown in Figure 4, after stimulus UV exposure, the LCE bends from the rear to the front side. Photo-isomerization of **AZO** changes the order parameter of the LC molecules. In this case, a decrease in the molecular order on the rear side increases the film length, leading to bending from the rear to the front

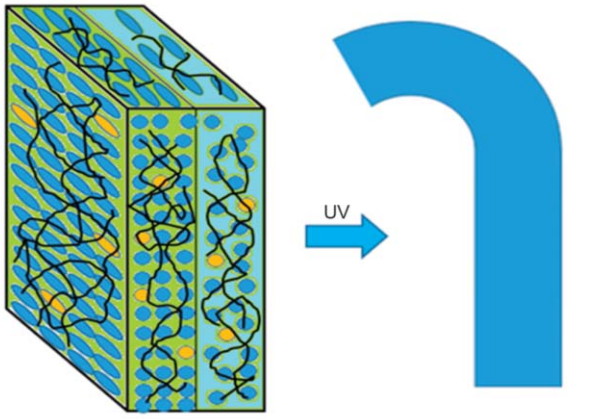

Figure 4. Photo-isomerization of **AZO** decreases the order parameter of LC molecules, leading to bending from the rear to the front side.

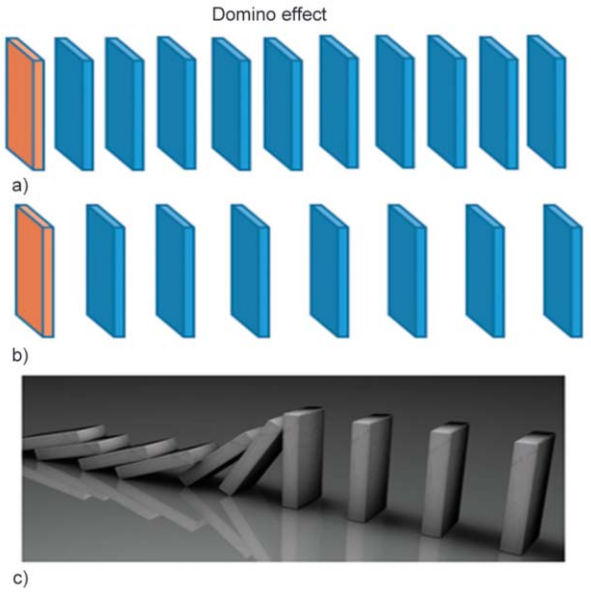

Figure 5. Effect of distance between pieces on the domino effect: (a) too close, (b) good arrangement, and (c) falling down smoothly.

side. Film bending is ascribed to the disturbance caused by trans-cis isomerization. The curved cis form of **AZO** may disturb the arrangement of molecules, leading to a decrease in the order parameter of the LC molecules. Figure 5 shows the relationship of distance on the domino effect. Figure 5a and Figure 5b show the arrangement of pieces with different distances. A proper distance is needed for the occurrence of the domino effect. Figure 5c shows the domino effect, displaying pieces falling down one by one. However, in the case of a crowded arrangement, as shown in Figure 6, the domino effect will not be observed. As shown in Figure 3 and Figure 4, the molecular arrangement on the front side is too crowded to induce the domino effect. The occurrence of the

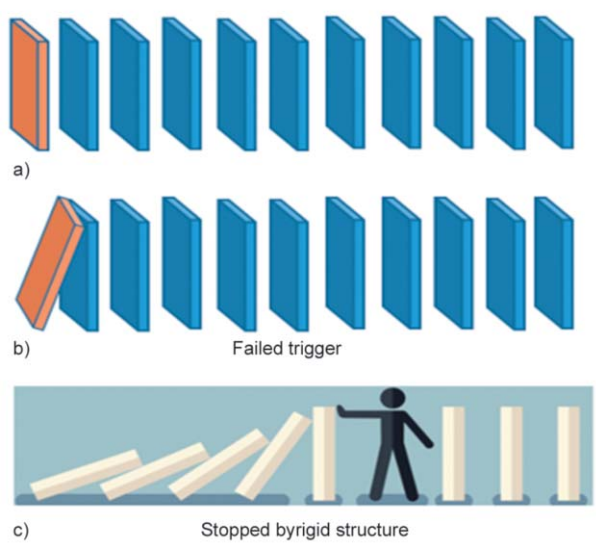

Figure 6. (a) Crowded domino pieces, (b) crowded pieces failing to start the domino effect, and (c) the domino effect stopped by a rigid construction.

domino effect on the rear side causes a decrease in the order parameter, leading to the extension and shrinkage of the sample films.

3.3. Effect of photo-isomerization

Figure 7a shows the domino effect of the trans-cis isomerization of **AZO** on the molecular arrangement. Figure 7b shows a real example of UV-triggered bending of a strip of film. As shown in Figure 8a and 8b, trans-cis isomerization changed the **AZO** molecule from a linear to a curved shape, resulting in real film shrinkage that led to the bending of the strip sample film. The phenomena are similar to the case shown in Figure 3b. In addition, with respect to the UV strength, as shown in Figure 8c, a higher UV power disturbs molecules more effectively, leading to more curling. Figure 9 shows a comparison of Figure 9a natural mimosa, and Figure 9b the fabricated

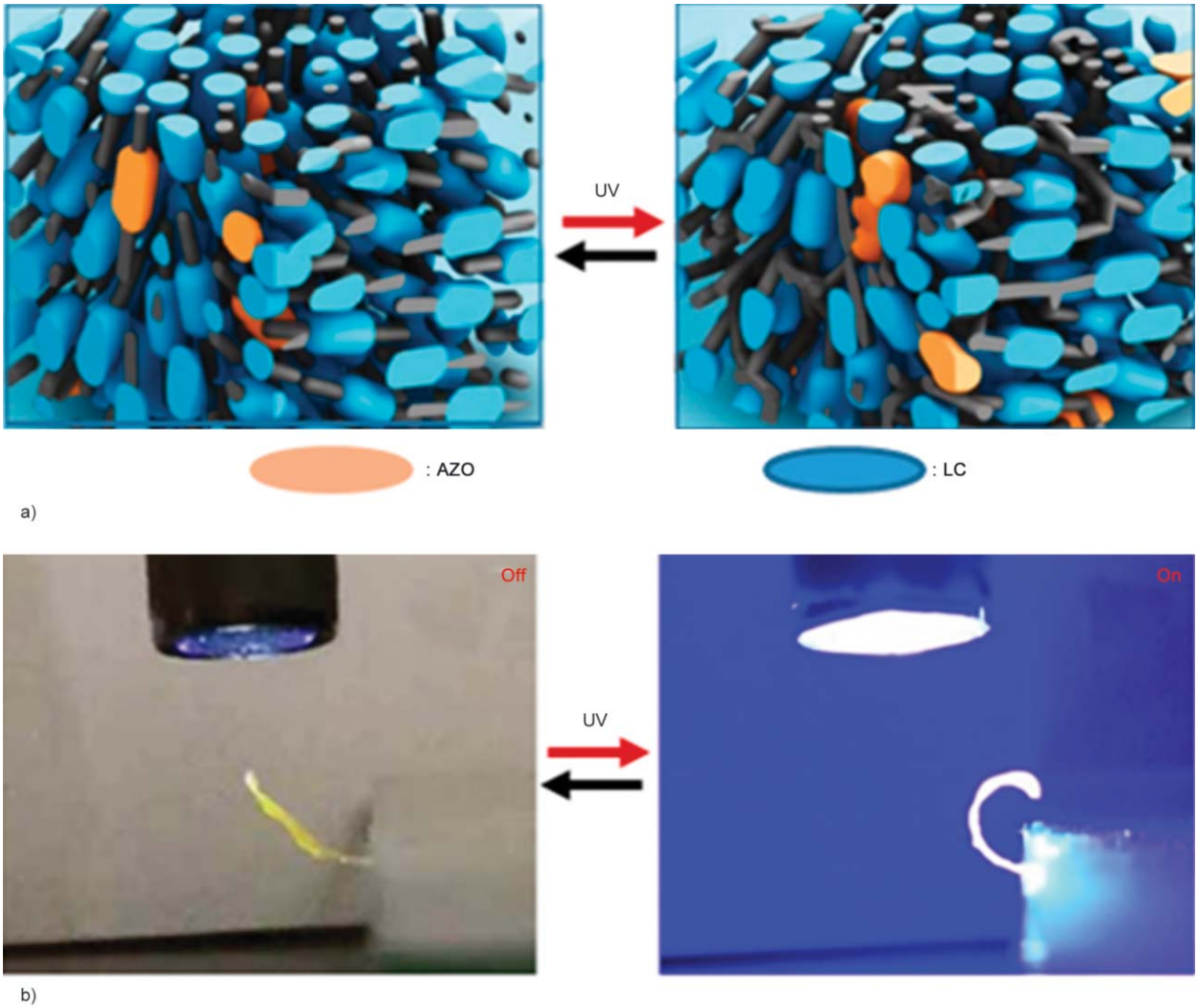

Figure 7. (a) Variation in molecular arrangement before and after light exposure and (b) bending of the synthesized LCE sample film before and after UV exposure.

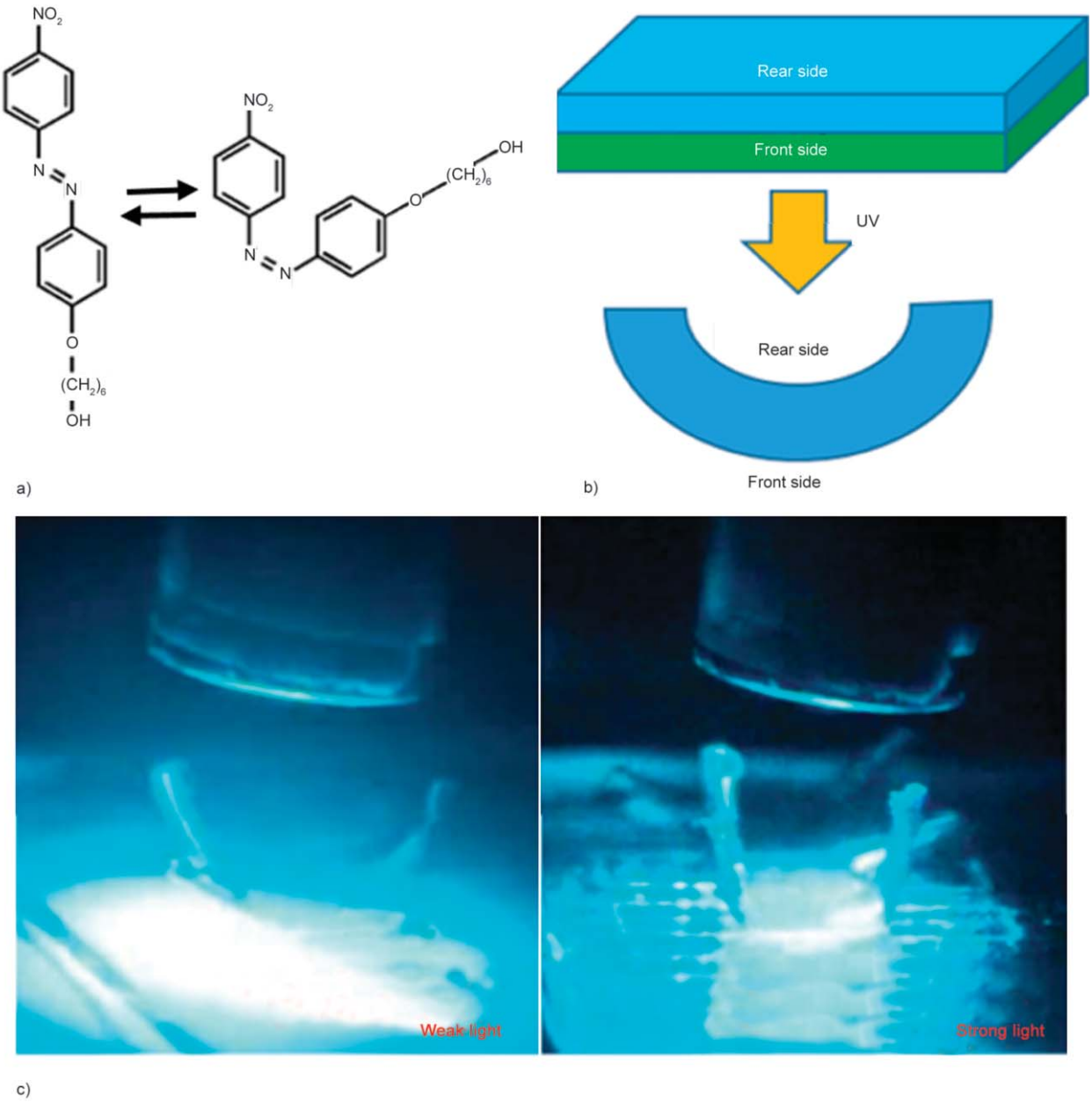

Figure 8. (a) Trans-cis isomerization of the **AZO** compound, (b) film curved to the rear side during light irradiation, and (c) response of the synthesized LCEs exposed to light.

liquid crystal film. To simulate natural mimosa, the synthesized liquid crystal film was cut into multi-toothed shapes, as shown in Figure 9c. The photo-stimulated curling was observed.

3.4. Sensitivity and stability of LCEs

To investigate the performance of the fabricated liquid crystal actuator, various wavelengths of exposure light ranging from 254 nm (UV light) to 633 nm (red light) were used. Blue light-emitting diodes with a wavelength of 405 nm and intensity of 15 mW/cm^2 induce a significant response of the fabricated LCEs. Figure 10a shows the real action of the light-stimulated LCE before and after light exposure. Figure 10b shows the estimation of the bending angle during stimulus light exposure. To increase the illumination rate, 365 nm UV light (91 mW/cm^2) was used, and the film was bent from an initial state ($\theta = 163°$) to $\theta = 72°$. In the absence of UV light, the irradiated LCE actuator recovered to its original shape. Furthermore, the dependence of the light wavelength and light intensity on the bending angle are shown in Figure 10c. Both shorter wavelengths of 365 and 325 nm show higher efficiency, indicating that an increase in light intensity increases the bending angle. Figure 10d shows the stability of the stimulated action of the synthesized LCE. After 30 stimulation cycles, the sample film showed no significant decay of

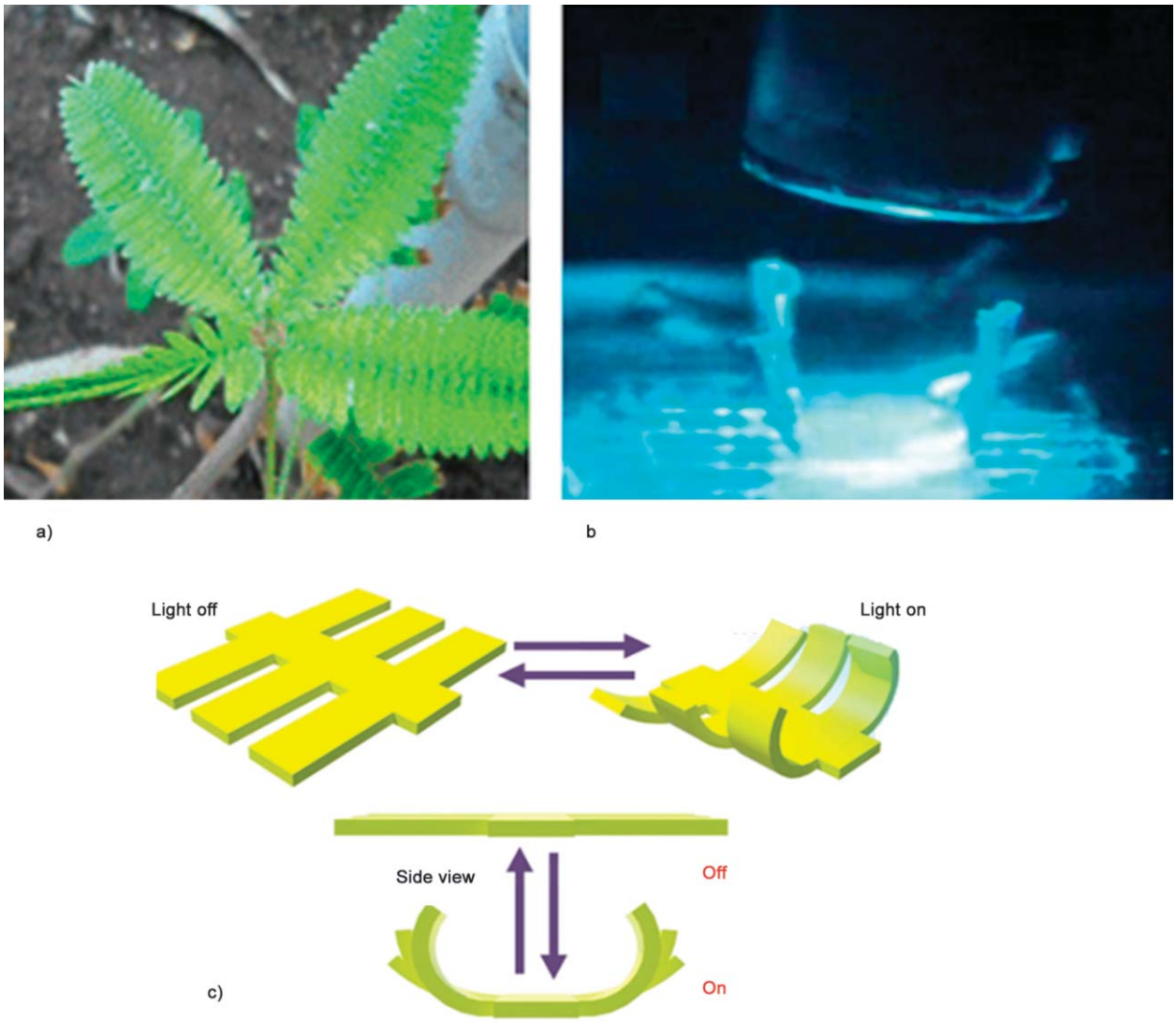

Figure 9. (a) Natural mimosa, (b) the synthesized multi-toothed sample film, and (c) schematic representation of the film response triggered by UV light.

the bending angle. In Figure 10d, 365 nm UV light (91 mW/cm^2) was used for the estimation. The measurement was carried out at room temperature (25 °C).

Considering the polymerization of the liquid-crystal mixture in the polymerization cell, photoinduced polymerization occurred once the mixture was exposed to UV light. Theoretically, due to the difference in copolymerization rates, the polymer components should be different depending on the location of the film from top to bottom. Higher UV energy in the top zone of the LC mixture results in efficient polymerization leading to higher polymer density. On the bottom side, the area could be considered a weak UV energy zone. In addition, the **AZO** dye in the liquid-crystal mixture absorbs light, leading to continuously decreasing UV energy from top to bottom. This effect could be the reason why the SEM morphologies of both sides exhibit different polymer densities.

4. Conclusions

In conclusion, we demonstrate the fabrication of mimosa-mimetic LCEs based on two predesigned liquid-crystal monomers with different reaction rates via gradient-controlled UV polymerization. The fabricated LCE polymer films show light-sensitive bending activity. The stability of repeated photosensitive bending actions was confirmed. This study opens a new opportunity to fabricate films that can show photostimulated bending in controlled directions via the domino effect. These mimosa-mimetic films are expected to find applications in the field of micro-robotics and micromachinery. Currently, enhancing the photo/near-IR sensitivity of the synthesized LCEs via polydopamine is now in progress.

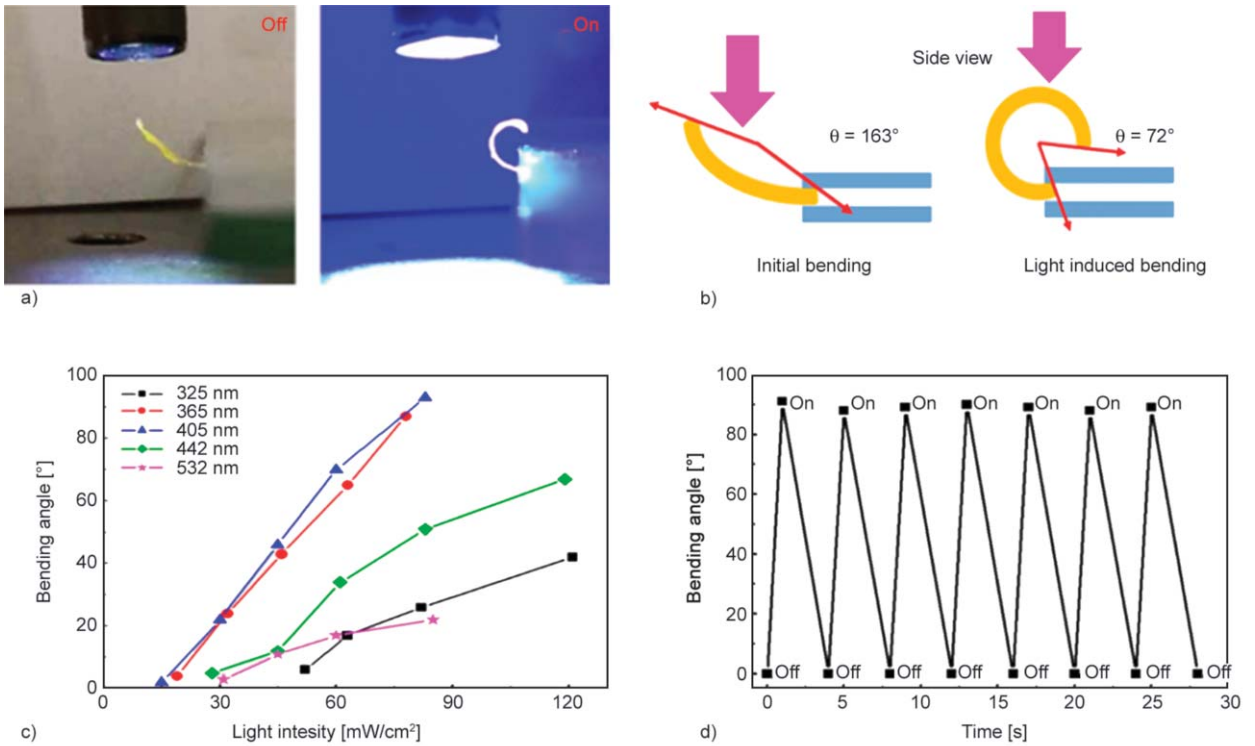

Figure 10. (a) Before and after light exposure, (b) estimation of bending angle, (c) dependence of bending angle on light intensity with various wavelengths, and (d) stability of repeated actuation cycles.

References

[1] Wani M., Zeng H., Priimagi A.: A light-driven artificial flytrap. Nature Communications, **8**, 15546/1–15546/7 (2017). https://doi.org/10.1038/ncomms15546

[2] Wegst U. G., Bai H., Saiz E., Tomsia A. P.: Ritchie R. O.: Bioinspired structural materials. Nature Materials, **14**, 23–36 (2015). https://doi.org/10.1038/nmat4089

[3] Rossin K. J.: Biomimicry: Nature's design process versus the designer's process. Design and Nature V, **138**, 559–570 (2010). https://doi.org/10.2495/dn100501

[4] Purkait M. K., Sinha M. K., Mondal P., Singh R.: Biologically responsive membranes. Interface Science and Technology, **25**, 145–171 (2018). https://doi.org/10.1016/B978-0-12-813961-5.00005-X

[5] Morris E., Chavez M., Tan C.: Dynamic biomaterials: Toward engineering autonomous feedback. Current Opinion in Biotechnology, **39**, 97–104 (2016). https://doi.org/10.1016/j.copbio.2016.02.032

[6] Cully A., Clune J., Tarapore D., Mouret J-P.: Robots that can adapt like animals. Nature, **521**, 503–507 (2015). https://doi.org/10.1038/nature14422

[7] Ma K. Y., Chirarattananon P., Fuller S. B., Wood R. J.: Controlled flight of a biologically inspired, insect-scale robot. Science, **340**, 603–607 (2013). https://doi.org/10.1126/science.1231806

[8] Speck O., Speck T.: An overview of bioinspired and biomimetic self-repairing materials. Biomimetics, **4**, 1–34 (2019). https://doi.org/10.3390/biomimetics4010026

[9] Kim H. G., Jeong K., Seo T. W.: Analysis and experiment on the steering control of a water-running robot using hydrodynamic forces. Journal of Bionic Engineering, **14**, 34–46 (2017). https://doi.org/10.1016/S1672-6529(16)60376-1

[10] Morin S. A., Shepherd R. F., Kwok S. W., Stokes A. A., Nemiroski A., Whitesides G. M.: Camouflage and display for soft machines. Science, **337**, 828–832 (2012). https://doi.org/10.1126/science.1222149

[11] Tottori S., Zhang L., Qiu F., Krawczyk K. K., Franco-Obregon A., Nelson B. J.: Magnetic helical micromachines: Fabrication, controlled swimming, and cargo transport. Advanced Materials, **24**, 811–816 (2012). https://doi.org/10.1002/adma.201103818

[12] Gershman S. J., Horvitz E. J., Tenenbaum J. B.: Computational rationality: A converging paradigm for intelligence in brains, minds, and machines. Science, **349**, 273–278 (2015). https://doi.org/10.1126/science.aac6076

[13] García C. G., Meana-Llorián D., Bustelo G., Cueva-Lovelle J. M.: A review about smart objects, sensors, and actuators. International Journal of Interactive Multimedia and Artificial Intelligence, **4**, 7–10 (2017). https://doi.org/10.9781/ijimai.2017.431

[14] Lashgari S., Karrabi M., Ghasemi I., Azizi H., Messori M., Paderni K.: Shape memory nanocomposite of poly (L-lactic acid)/graphene nanoplatelets triggered by infrared light and thermal heating. Express Polymer Letters, **10**, 349–359 (2016). https://doi.org/10.3144/expresspolymlett.2016.32

[15] Maksimkin A. V., Kaloshkin S. D., Zadorozhnyy M. V., Senatov F. S., Salimon A. I., Dayyoub T.: Artificial muscles based on coiled UHMWPE fibers with shape memory effect. Express Polymer Letters, **12**, 1072–1080 (2018). https://doi.org/10.3144/expresspolymlett.2018.94

[16] Szmechtyk T., Sienkiewicz N., Strzelec K.: Thermally induced self-healing epoxy/glass laminates with porous layers containing crystallized healing agent. Express Polymer Letters, **12**, 640–648 (2018). https://doi.org/10.3144/expresspolymlett.2018.54

[17] Ji W. F., Li C. W., Yu S. K., Chen P. J., Chen H. L., Chen R. D., Chen B. H., Hsu C. L., Yeh J. M.: Biomimetic electroactive polyimide with rose petal-like surface structure for anticorrosive coating application. Express Polymer Letters, **11**, 635–644 (2017). https://doi.org/10.3144/expresspolymlett.2017.61

[18] Park K. H., Kim S. J., Hwang M. J., Song H. J., Park Y. J.: Biomimetic fabrication of calcium phosphate/chitosan nanohybrid composite in modified simulated body fluids. Express Polymer Letters, **11**, 14–20 (2017). https://doi.org/10.3144/expresspolymlett.2017.3

[19] Shang J., Le X., Zhang J., Chen T., Theato P.: Trends in polymeric shape memory hydrogels and hydrogel actuators. Polymer Chemistry, **10**, 1036–1055 (2019). https://doi.org/10.1039/c8py01286e

[20] Zou Y., Lam A., Brooks D. E., Phani A. S., Kizhakkedathu J. N.: Bending and stretching actuation of soft materials through surface initiated polymerization. Angewandte Chemie, **123**, 5222–5225 (2011). https://doi.org/10.1002/ange.201008252

[21] Saha S., Copic D., Bhaskar S., Clay N., Donini A., Hart A. J., Lahann J.: Chemically controlled bending of compositionally anisotropic microcylinders. Angewandte Chemie International Edition, **51**, 660–665 (2012). https://doi.org/10.1002/anie.201105387

[22] Kamal T., Park S-Y.: Shape-responsive actuator from a single layer of a liquid-crystal polymer. ACS Applied Materials Interfaces, **6**, 18048–18054 (2014). https://doi.org/10.1021/am504910h

[23] Ziółkowski B., Diamond D.: Thermoresponsive poly (ionic liquid) hydrogels. Chemical Communications, **49**, 10308–10310 (2013). https://doi.org/10.1039/c3cc45862h

[24] Rogóż M., Zeng H., Xuan C., Wiersma D. S., Wasylczyk P.: Light-driven soft robot mimics caterpillar locomotion in natural scale. Advanced Optical Materials, **4**, 1689–1694 (2016). https://doi.org/10.1002/adom.201600503

[25] Ikeda T., Mamiya J-I., Yu Y.: Photomechanics of liquid-crystalline elastomers and other polymers. Angewandte Chemie International Edition, **46**, 506-528 (2007). https://doi.org/10.1002/anie.200602372

[26] Ohm C., Brehmer M., Zentel R.: Liquid crystalline elastomers as actuators and sensors. Advanced Materials, **22**, 3366–387 (2010). https://doi.org/10.1002/adma.200904059

[27] Li M-H., Keller P., Li B., Wang X., Brunet M.: Light-driven side-on nematic elastomer actuators. Advanced Materials, **15**, 569–572 (2003). https://doi.org/10.1002/adma.200304552

[28] Raven P. H.: Biology of plants. Freeman, New York (2005).

[29] Driessche T. V.: Nutations in shoots and in desmodium lateral leaflets, nyctinastism and seismonastism in *Mimosa pudica*. Comparison and evolution of morphology and mechanism. Biological Rhythm Research, **31**, 451–468 (2000). https://doi.org/10.1076/0929-1016(200010)31:4;1-2;ft451

[30] van Oosten C. L., Bastiaansen C. W. M., Broer D. J.: Printed artificial cilia from liquid-crystal network actuators modularly driven by light. Nature Materials, **8**, 677–682 (2009). https://doi.org/10.1038/nmat2487

[31] Camacho-Lopez M., Finkelmann H., Palffy-Muhoray P., Shelley M.: Fast liquid-crystal elastomer swims into the dark. Nature Materials, **3**, 307–310 (2004). https://doi.org/10.1038/nmat1118

[32] Zeng H., Wani O. M., Wasylczyk P., Priimagi A.: Self-regulating iris based on light-actuated liquid crystal elastomer. Advanced Materials, **29**, 1701814/1–1701814/7 (2017). https://doi.org/10.1002/adma.201701814

[33] Kamal T., Park S-Y.: Shape-responsive actuator from a single layer of a liquid-crystal polymer. ACS Applied Materials Interfaces, **6**, 18048–18054 (2014). https://doi.org/10.1021/am504910h

[34] Liu J-H., Chiu Y-H.: Process equipped with a sloped UV lamp for the fabrication of gradient-refractive-index lenses. Optical Letters, **34**, 1393–1395 (2009). https://doi.org/10.1364/ol.34.001393

[35] Zhang Y-S., Emelyanenko A. V., Liu J-H.: Fabrication and optical characterization of imprinted broad-band photonic films via multiple gradient UV photopolymerization. Journal of Polymer Science Part B: Polymer Physics, **55**, 1427–1435 (2017). https://doi.org/10.1002/polb.24392